scientific reports

Check for updates

OPEN

Fe_3O_4@SiO_2/Schiff-base/Zn (II) nanocomposite functioning as a versatile antimicrobial agent against bacterial and fungal pathogens

Sedigheh Azadi[1], Ali Mohammad Amani[1]✉, Ali Jangjou[2], Ahmad Vaez[3], Zahra Zareshahrabadi[4], Aylin Zare[1,2], Seyed Reza Kasaee[5], Hesam Kamyab[6,7]✉, Shreeshivadasan Chelliapan[8] & Sareh Mosleh-Shirazi[9]

Antimicrobial resistance (AMR) presents a critical global health issue, necessitating novel therapeutic strategies to manage bacterial and fungal infections. This study explores the development and evaluation of multifunctional Fe_3O_4@SiO_2/Schiff-base/Zn (II) magnetic nanocomposite (MNC) with enhanced antimicrobial properties. The synthesized MNC combines the magnetic characteristics of Fe_3O_4 magnetic nanoparticles (MNPs) with the antimicrobial properties of Schiff-base ligand functionalized with Zn (II) ions. The preparation involved the coprecipitation of Fe_3O_4, coating with SiO_2 via a modified Stöber method, and subsequent functionalization with Schiff-base/Zn (II) complex. Comprehensive characterization using FT-IR, XRD, SEM, TEM, DLS, EDX, VSM, and TGA confirmed successful synthesis, structural integrity, and superparamagnetic behavior of the MNPs and MNC. The antifungal and antibacterial activities were assessed against six *Candida* species and four bacterial strains using broth microdilution methods. The Fe_3O_4@SiO_2/Schiff-base/Zn (II) MNC exhibited significant inhibitory effects, with MIC values of 8–64 µg/mL for *Candida* species and 64–512 µg/mL for bacteria, demonstrating potent antimicrobial efficacy. The MTT assay indicated biocompatibility across various concentrations, except for slight cytotoxicity at 256 µg/mL after five days. To our knowledge, this is the first report integrating Zn (II) Schiff-base ligands into magnetic nanoparticles to achieve a versatile platform for both antimicrobial and biofilm inhibition applications.

Keywords Candida Species, Anti-fungal property, Anti-bacterial property, Biofilm Inhibition, Cytotoxicity

Antimicrobial resistance (AMR) is still an important worldwide health issue that makes managing infectious illnesses much more challenging and puts decades of improvements in medical treatment at risk[1]. There is an urgent need for new treatment approaches since the emergence of resistance in bacterial and fungal infections has raised morbidity, mortality, and healthcare expenses[2]. Historically, the cornerstone for treating infections has been conventional antimicrobial medicines, such as antibiotics and antifungal drugs. Antibiotics that are often used include beta-lactams (like penicillins and cephalosporins), macrolides (like azithromycin), and

[1]Department of Medical Nanotechnology, School of Advanced Medical Sciences and Technologies, Shiraz University of Medical Sciences, Shiraz, Iran. [2]Department of Emergency Medicine, School of Medicine, Namazi Teaching Hospital, Shiraz University of Medical Sciences, Shiraz, Iran. [3]Department of Tissue Engineering and Applied Cell Sciences, School of Advanced Medical Sciences and Technologies, Shiraz University of Medical Sciences, Shiraz, Iran. [4]Basic Sciences in Infectious Diseases Research Center, Shiraz University of Medical Sciences, Shiraz, Iran. [5]Shiraz Endocrinology and Metabolism Research Center, Shiraz University of Medical Sciences, Shiraz, Iran. [6]Department of Biomaterials, Saveetha Dental College, and Hospital, Saveetha Institute of Medical and Technical Sciences, Chennai 600077, India. [7]The KU-KIST Graduate School of Energy and Environment, Korea University, 145 Anam-Ro, Seongbuk-Gu, Seoul 02841, Republic of Korea. [8]Department of Smart Engineering and Advanced Technology, Faculty of Artificial Intelligence, Universiti Teknologi Malaysia, Jalan Sultan Yahya Petra, Kuala Lumpur 54100, Malaysia. [9]Department of Materials Science and Engineering, Shiraz University of Technology, Shiraz, Iran. ✉email: amani_a@sums.ac.ir; hesam_kamyab@yahoo.com

fluoroquinolones (like ciprofloxacin)[3]. These medications work by interfering with vital bacterial functions such as DNA replication, protein synthesis, and cell wall creation[4].

However, the advent of resistance bacteria places serious restrictions on these medications. For example, many conventional antibiotics are no longer effective against methicillin-resistant Staphylococcus aureus (MRSA) and extended-spectrum beta-lactamase (ESBL)-producing Enterobacteriaceae, which results in higher treatment failure rates and more severe infections[5,6]. Also, treating fungal infections is becoming more difficult since fungi like Candida auris are becoming more resistant to antifungal drugs like azoles (like fluconazole) and echinocandins (like caspofungin)[7].

Despite various advancements in nanoparticle-based treatments, the integration of multifunctional properties, such as targeted antimicrobial activity and magnetic recoverability, remains underexplored. In light of these challenges, nanoparticles (NPs) have emerged as a potential class of materials that provide novel solutions for antimicrobial treatment[8]. NPs, particularly those with high surface area-to-volume ratios like silver, copper, and zinc oxide NPs, have unique antibacterial mechanisms[9]. These include the release of reactive oxygen species (ROS), and disruption of the membrane and microbial metabolic pathways[9,10]. Their capacity to permeate microbial cells and interact with intracellular components improves efficacy against both resistant bacterial and fungal strains[11]. Furthermore, NPs' ability to be functionalized with multiple ligands or coatings allows for the modification of antimicrobial features and improved effectiveness[12].

Iron oxide NPs (Fe_3O_4) are known for their superparamagnetic characteristics, which facilitate separation and recovery using external magnetic fields[13,14]. Wrapping the magnetic core of Fe_3O_4 with a silica (SiO_2) shell improves stability, biocompatibility, and effectiveness[15]. This core-shell structure not only increases the mechanical strength of the NPs, but it acts as a flexible framework for additional functionalization. In this regard, Schiff base complexes bearing azomethine groups (-C = N), formed by the chemical reaction of an amine and a carbonyl compound, can be used to modify Fe_3O_4@SiO_2 NPs[16]. This modification improves their antibacterial capabilities and enables targeted applications in the treatment of resistant microbial diseases. The addition of Schiff base complexes enhances the NPs ' stability and bioavailability, making them more efficient against a wide spectrum of pathogens by interfering with microbial enzymatic activity and cellular processes[17].

The tunability of both the Schiff base ligands and the choice of metal ions allows for the optimization of antimicrobial potency against a variety of bacterial and fungal strains, making them promising candidates for the development of new antimicrobial agents. Various metal Schiff-base complexes have been reported exhibiting antimicrobial activities such as Cd (II)[18,19], Co (II)[20], Cu (II)[21–24], Ni (II)[20,23,25], Fe (II)[23,26], and Fe (III)[27]. Furthermore, different Schiff-base complexes of Zn have been synthesized and showed antimicrobial activities, some of which are presented in Scheme 1. Zn complex of (*E*)-2-(((7-chloro-2-hydroxyquinolin-3-yl) methylene) amino)-3-phenylpropanoic acid (Scheme 1A)[28], Zn Schiff-base complexes of 3 ligands of 2-chloro-6-((5-chloro-2-hydroxybenzylidene)amino)-4-nitrophenol, 2,4-dibromo-6-(((3-chloro-2-hydroxy-5 nitrophenyl)imino) methyl)phenol, and 2-chloro-6-((2-hydroxy-3-methyl-5-nitrobenzylidene)amino)-4-nitrophenol (Scheme 1B)[20], Zn (II) complex of schiff bases based-on glycine and phenylalanine (Scheme 1C)[29], symmetrical Schiff base complex zinc(II) prepared via the condensation reaction of 2,2′-diamino-4,4′-dimethyl-1,1′-biphenyl or 2,2′-diamino-6,6′-dibromo-4,4′-dimethyl-1,1′-biphenyl with 3,5-dichloro- or 5-nitro salicylaldehyde (Scheme 1D)[26], Zn (II) complex with ONNO donor Salen-type Schiff base ligands, derived from different 3,5-dihalosalicylaldehyde with polymethylenediamines of varying chain length (Scheme 1E)[25], Zn (II) Complex with (E)-2-((5-Bromothiazol-2-yl)imino)methyl)phenol Ligand (Scheme 1F)[30], Zn (II) complex with Schiff bases derived from trimethylsilyl-propyl-*p*-aminobenzoate (Scheme 1G)[31], Zn (II) complex of 5-aminobenzofuran-2-carboxylate Schiff base ligands (Scheme 1H)[22], Zn complex of [(1E,1′E)-N, N′-(1,2-phenylene)bis (1-(5-(2 fluorophenyl)furan-2-yl)methanimine) (Scheme 1I)[32], Zn (II) complex of 4-[(5-oxo-4,5-dihydro-1,3-thiazol-2-yl)hydrazono]methyl}phenyl-4-methylbenzenesulfonate Schiff-base ligand (Scheme 1J)[27].

Zinc [Zn (II)] has received attention among metal ions used in Schiff base complexes due to its varied role in biological systems and potent antibacterial properties[32]. Zn (II) ions are known to have antimicrobial properties by disrupting microbial enzyme functions, restricting nucleic acid synthesis, and generating ROS, all of which lead to microbial cell death[20]. More importantly, the incorporation of Zn (II) into the Schiff-base-functionalized silica shell of Fe_3O_4 NPs could result in a synergistic effect that combines magnetic separation ability with increased antibacterial and antifungal activity. These hybrid materials are predicted to provide considerable benefits in targeted biomedical applications such as the Schiff base complex of Cu (II) supported on Fe_3O_4/SiO_2/APTS[21].

Schiff-base metal complexes, particularly those based on zinc, have been widely studied due to their antimicrobial properties. However, the integration of magnetic functionality with antimicrobial activity remains underexplored. Previous studies have primarily focused on improving the antimicrobial efficacy of these complexes, without considering the added benefit of magnetic responsiveness. Also, the magnetic core nanoparticles functionalized with Schiff base complexes have been widely used as heterogenous catalysts in organic reactions and a few studies focused on antimicrobial properties. For example, the synthesis of N_4-donor Schiff base copper (II) immobilized on superparamagnetic Fe_3O_4@SiO_2 as a recyclable catalyst for oxidation reactions and an antibacterial agent[33], synthesis of Ni (II), Cu (II), Fe (II) and Fe_3O_4 NP complexes with tetraaza macrocyclic Schiff base ligand for antimicrobial activity[23], and Fe_3O_4@SiO_2-Schiff base-Pd(II) for synthesis of 12*H*-benzo[5,6]chromeno[2,3-b]pyridine-10-carbonitriles and evaluation of antibacterial activity[34].

As a continuous of our research in the area of Schiff-base complexes, NPs, and antimicrobial studies, and our previous antifungal report based on Cu NPs[35], we present a Schiff-base/Zn (II) complex that not only exhibits enhanced antimicrobial activity but also possesses magnetic properties, allowing for potential applications in magnetic targeting for drug delivery. This dual functionality is achieved through a novel synthesis route that enhances both the stability and performance of the complex, making it a promising candidate for advanced biomedical applications. The integration of Zn (II) Schiff-base complexes into a Fe_3O_4@SiO_2 core-shell

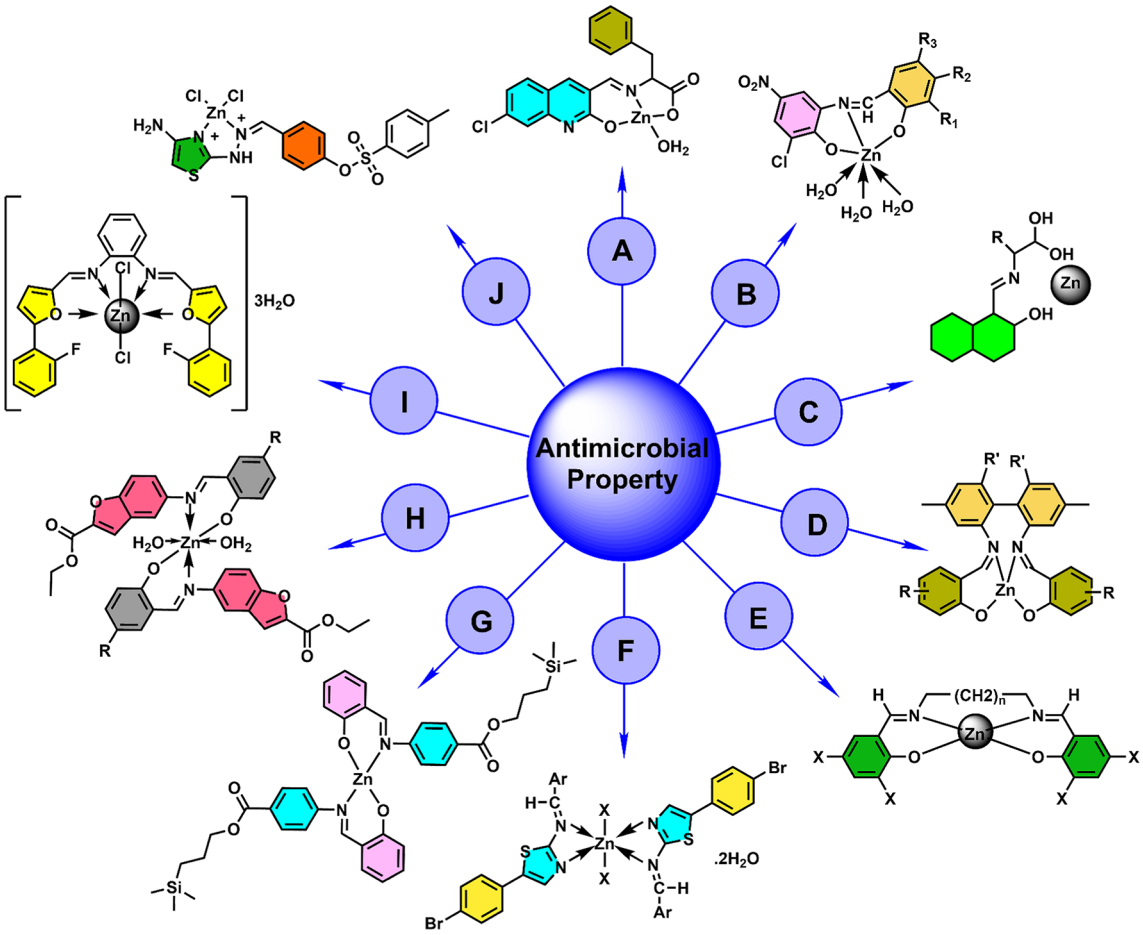

Scheme 1. Different Schiff-base ligands of Zn metal exhibiting antimicrobial activity.

nanostructure creates a multifunctional material with synergistic antimicrobial properties. This hybrid system uniquely combines the advantages of magnetic recoverability, enhanced biofilm inhibition, and broad-spectrum antimicrobial activity.

Materials and methods

The following chemicals were purchased from Sigma-Aldrich to synthesize Fe_3O_4@SiO_2/Schiff-base/Zn (II) MNC: Iron (III) chloride hexahydrate [$FeCl_3.6H_2O$], Iron (II) chloride tetrahydrate [$FeCl_2.4H_2O$], cetyltrimethylammonium bromide (CTAB), Tetraethyl orthosilicate (TEOS), 3-aminopropyltriethoxysilane (APTES), sodium hydroxide (NaOH), 2-hydroxy benzaldehyde (salicylaldehyde), and zinc (II) acetate dihydrate [Zn $(OAc)_2$. $2H_2O$]. Potassium bromide (KBr), The materials for the MTT assay as (3-(4,5-Dimethylthiazol-2-yl)-2,5-Diphenyltetrazolium Bromide). Solvents like Dimethyl Sulfoxide (DMSO), Ethanol (EtOH) were bought from Merk company (Germany). Deionized water was obtained from the EC model: DWB RO-LAB. The solvents were used with no more purification.

The Fe_3O_4@SiO_2/Schiff-base/Zn (II) MNC was successfully synthesized and characterized using both quantitative and qualitative analytical techniques. A Tensor II spectrophotometer (Brucker company) was used to record the materials' FT-IR spectra. The crystalline structure and phase composition of MNPs and MNC were examined by XRD analysis using a Bruker AXS D8-Advance X-ray diffractometer with Cu Kα radiation (λ = 1.5418). The elements of materials were characterized using EDX. A BHV-55 VSM was used to measure the magnetization of NPs using the VSM technique. Using a NETZSCH STA 409 PC/PG, TGA assessed the NPs' thermal stability. A Philips EM208 transmission electron microscope running at 80 kV accelerating voltage captured the TEM image, while TESCAN-Vega3 captured the SEM image. Using a HORIBA-SZ 100, the DLS technique was used to measure the NPs' size distribution and zeta potential. The UV-Vis spectrum was recorded by a microplate reader (BMG Labtech, Berlin, Germany).

Synthesis of Fe_3O_4@SiO_2/Schiff-base/Zn (II)

The coprecipitation method was used to produce Fe_3O_4 MNPs. First, a mixture of $FeCl_3.6H_2O$ (1.3 g, 4.0 mmol), $FeCl_2.4H_2O$ (0.9 g, 4.5 mmol), and CTAB (1.0 g) as a surfactant was added to a beaker containing deionized water (600 cm^3) and stirred mechanically for 0.5 h at 80 °C under N_2 conditions. Next, 10% NaOH was added dropwise while vigorously stirring to create a solid black product. This process continued until the reaction

medium reached pH 10–12. The black magnetic Fe_3O_4 product was heated at 60 ˚C for 2 h, after which it was magnetically separated and washed three times with ethanol and deionized water[16].

Using a modified Stöber approach, the core-shell Fe_3O_4@SiO_2 MNPs were produced. Dropwise addition of NaOH 10% w (5.0 cm^3) was done after adding Fe_3O_4 (0.5 g) to a beaker containing EtOH (50.0 cm^3), deionized water (5.0 cm^3), and (TEOS) (0.2 cm^3, 1.0 mmol). The Fe_3O_4@SiO_2 product was stirred at room temperature for half an hour, and then it was washed with ethanol and deionized water before being dried for 10 h at 80 ˚C[35].

On the other side, the Schiff-base ligand was synthesized in the next step, and then the Zn metal ions were anchored. In this regard, the Schiff base ligand was formed during the 6-hour reaction between (APTES) (1.0 mmol) and salicylaldehyde (1.0 mmol) in EtOH (50.0 cm^3) at room temperature. After being washed with ethanol, the yellow solid Schiff-base ligand was vacuum-dried[1]. H NMR (250 MHz, $CDCl_3$): δ = 0.7 (t, 2 H, CH_2, J = 8.5 Hz); 1.22 (t, 9 H, CH_3, J = 7.0 Hz); 1.82 (m, 2 H, CH_2); 3.59 (t, 2 H, CH_2, J = 6.5 Hz); 3.81 (q, 6 H, CH_2, J = 7.0 Hz); 6.85–6.96 (m, 2 H, CH aromatic); 7.21–7.29 (m, 2 H, CH aromatic); 8.33 (s, 1 H, CH); 13.59 (s, 1 H, OH)[36].

Then, Zn $(OAc)_2$. $2H_2O$ (1.0 mmol) and Schiff-base ligand (2.0 mmol) in EtOH (25.0 cm^3) were mixed under reflux conditions to create the Schiff-base complex of Zn (II), which was produced as a green compound. Finally, the synthesis of Fe_3O_4@SiO_2/Schiff-base/Zn (II) was performed after 12 h of heating the mixture of Schiff-base complex of Zn (II) (1.0 mmol) and Fe_3O_4@SiO_2 (2.0 g) in EtOH (10.0 cm^3) under reflux conditions. After being separated by an external magnet, the product was washed with ethanol and water and dried for 6 h at 80 ˚C.

Antifungal measurement of Fe_3O_4@SiO_2/Schiff-base/Zn (II) by broth microdilution method

The minimum inhibitory concentrations (MIC) and the minimum fungicidal concentration (MFC) for the six primary *Candida* (*C.*) fungal species, were determined using the broth microdilution method. Inocula for the tested yeast fungi species from Centraal bureau voor Schimmelcultures (CBS) and American Type Culture Collection (ATCC), *C. albicans* (C 562), *C. glabrata* (A 90,030), *C. dubliniensis* (C 8501), *C. krusei* (A 6258), *C. tropicalis* (A 750), and *C. parapsilosis* (A 4344) strains, were prepared from 24-hour cultures. These fungal suspensions were adjusted to a standard turbidity level of 0.5 McFarland, equivalent to a stock suspension of $1–5 \times 10^6$ cells/mL. To assess antifungal activity, serial dilutions of Fe_3O_4@SiO_2/Schiff-base/Zn (II) (ranging from 0.5 to 256 µg/mL) were prepared in RPMI-1640 medium within 96-well microtiter plates. Subsequently, 100 µl of the prepared inoculums of the tested yeast fungi were added to the microtiter plates and incubated in a humid atmosphere (32 ˚C, 24–48 h). As controls, the culture medium alone and culture medium with yeast inoculums were utilized as the blank and growth controls, respectively. Each experiment was conducted in triplicate. Following the incubation time, the growth control and the growth in the 96-well microtiter plates were compared. The MIC was determined as the lowest concentration at which no noticeable growth occurred in the treatments provided. Furthermore, 10 µL of medium from wells that showed no visible yeast fungal growth on Sabouraud Dextrose Agar (SDA) was evaluated to determine the minimum fungicidal concentration (MFC). The MFC was defined as the lowest concentration at which no more than four colonies were observed, corresponding to a 99.9% mortality rate of the fungi in the initial inoculum[37]. The fluconazole served as a control in broth microdilution assay[38].

Antibacterial measurement of Fe_3O_4@SiO_2/Schiff-base/Zn (II) by broth microdilution method

The minimum inhibitory concentrations (MIC) and the minimum bactericidal concentration (MBC) of the Fe_3O_4@SiO_2@Schiff-base/Zn (II) MNC for standard species of bacteria including, *Staphylococcus aureus*, *Escherichia coli*, *Pseudomonas aeruginosa*, and *Enterococcus faecalis* were determined using the broth microdilution method. The inocula of tested bacteria species were prepared from 24 h cultures. Microbial suspensions were adjusted to 0.5 McFarland standard turbidity that is a stock suspension of $1–1.5 \times 10^8$ cells/ mL for bacteria. For the determination of antimicrobial activities, serial dilutions of the Fe_3O_4@SiO_2@Schiff-base/Zn (II) (0.25 to 128 µg/mL) were prepared in 96-well microtiter plates containing Mueller Hinton broth (MHB). Subsequently, 100 µL of the bacterial working inoculum was added to the microtiter plates and incubated under humid conditions at 37 °C for 24 h. The culture medium alone served as the negative control, while the culture medium containing bacterial inoculum was used as the growth control. Notably, all experiments were conducted in triplicate to ensure reliability and reproducibility of the results. Following the incubation period, microbial growth in the 96-well microtiter plates was assessed in comparison to the growth control. The lowest concentration of the tested treatments that exhibited no visible growth was defined as the MIC[39]. The cotrimoxazole served as a control in broth microdilution assay[38].

Antimicrobial activity by disk diffusion method

The antimicrobial activity of Fe_3O_4@SiO_2@Schiff-base/Zn (II) was evaluated using the disk diffusion method. Overnight cultures of microbial strains, including *Escherichia coli*, *Staphylococcus aureus*, *Pseudomonas aeruginosa*, and *Candida albicans*, were adjusted to a 0.5 McFarland standard to ensure uniformity. Mueller-Hinton agar plates were prepared and inoculated with the standardized microbial suspension. A solution of Fe_3O_4@SiO_2@Schiff-base/Zn (II) was prepared at a concentration of 32 µg/mL, and blank disks were immersed in this solution for 30 min. The treated disks were then placed on the inoculated agar plates. Following a 24-hour incubation at 37 °C, the inhibition zones around each disk were measured using a caliper or ruler. The recorded data provided a basis for assessing the antimicrobial efficacy of Fe_3O_4@SiO_2@Schiff-base/Zn (II) and allowed comparison with results obtained from the broth microdilution method.

Quantitative investigation of the antibiofilm activity

A quantitative analysis of the antibiofilm activity of Fe_3O_4@SiO_2@Schiff-base/Zn (II) was conducted using the 2,3-bis(2-methoxy-4-nitro-5-sulfo-phenyl)-2 H-tetrazolium-5-carboxanilide (XTT) reduction assay. Standard *Candida albicans* (C 562) was initially cultured on SDA plates. After a 24-hour incubation period, a single loopful of colonies was transferred into 20 mL of Sabouraud Dextrose Broth and incubated at 32 °C with continuous agitation (100 rpm) for 24 h. The resulting *C. albicans* suspension was washed twice with sterile phosphate-buffered saline (PBS; pH 7.2) and resuspended in RPMI 1640 medium. Cell concentrations were standardized to 1.0×10^6 cells/mL, as determined by spectrophotometric measurement at 530 nm. Serial dilutions of Fe_3O_4@SiO_2@Schiff-base/Zn (II) (ranging from 0.12 to 64 µg/mL) were prepared in RPMI 1640 medium within 96-well plates.

Subsequently, 100 µL of the *C. albicans* cell suspension was added to each well and incubated for 48 h to allow biofilm formation. Negative controls consisted of 200 µL of RPMI 1640 medium (blank), while positive controls contained RPMI 1640 medium with *C. albicans* but without treatment. The XTT solution (0.5 mg/mL, Sigma Chemical Co., St. Louis, USA) was prepared in Ringer's lactate, filter-sterilized (0.22 µm pore size), and stored at −70 °C. Before each assay, the XTT stock solution was combined with menadione sodium bisulfite (10 mM, Sigma Chemical Co., St. Louis, USA).

After the 48-hour incubation, biofilms were washed twice with sterile PBS, followed by the addition of 100 µL of the XTT/menadione solution to each well. The plates were incubated at 37 °C in the dark for 4 h. Colorimetric changes were measured at 570 nm using a microplate reader (BMG Labtech, Berlin, Germany). The inhibition percentage of *Candida* biofilm formation was calculated by comparing the absorbance values of treated samples to those of the positive control using the following equation[37].

$$\text{Biofilm inhibition } (\%) = \frac{\text{OD positive control} - \text{OD experimental}}{\text{OD positive control}} \times 100$$

The MTT assay

Using the MTT test, the cytotoxicity of the Fe_3O_4@SiO_2/Schiff-base/Zn (II) was quantified. The mouse L929 murine fibroblastic cell line was grown at 37 ˚C with CO_2 in a humidified incubator containing DMEM/F12 (1:1 mixture of Dulbecco's Modified Essential Medium (DMEM) and Ham's F-12 Medium) culture media supplemented with 10% (v/v) fetal bovine serum (FBS), 100 units/ml of penicillin, and 100 µg/ml of streptomycin. The cells were grown at a density of 5×10^3 cells per well in a 96-well cell culture plate. Each row had eight copies of sterilized Fe_3O_4@SiO_2/Schiff-base/Zn (II) MNC added at 64, 128, and 256 µg/mL. One row received no additional therapy, and this group was referred to as the control group. The culture media was withdrawn and 0.2 ml of MTT (0.5 mg/mL) was applied to each well at time points 1, 3, and 5 days after the cells were seeded. The cells were incubated at 37 ˚C for 4 h in a dark incubator. After that, the solution was discarded, and each well received 0.1 mL of DMSO to dissolve the formed formazan crystals. The samples' absorbance values and optical density (OD) were determined using a Biotech Instruments microplate reader at a wavelength of 570 nm[35].

Results and discussion

Synthesis of the Fe_3O_4@SiO_2/Schiff-base/Zn (II) MNC

As described in the experimental section, the preparation of Fe_3O_4@SiO_2/Schiff-base/Zn (II) is briefly shown in Fig. 1. First, the coating of the Fe_3O_4 core NPs being formed by the combination of Fe (II) and Fe (III) chloride salts was done by using the silica source of TEOS under pH control to afford Fe_3O_4@SiO_2 core-shell NPs. Second, the Schiff base complex of Zn (II) was made through the reaction between salicylaldehyde and APTES followed by adding Zn $(OAc)_2$. $2H_2O$. Finally, the Schiff base complex of Zn (II) was immobilized on the surface of Fe_3O_4@SiO_2 NPs under reflux conditions to obtain the Fe_3O_4@SiO_2/Schiff-base/Zn (II) MNC (Fig. 1).

Characterization of the Fe_3O_4@SiO_2/Schiff-base/Zn (II) MNC

FT-IR analysis

The characteristic chemical bonds in the structures are shown by the FT-IR spectra of (a) Fe_3O_4, (b) Fe_3O_4@SiO_2, (c) 2-((3-(triethoxysilyl)propyl)imino)methyl)phenol (Schiff-base ligand), (d) Zn (II)-Schiff-base complex, and (e) Fe_3O_4@SiO_2/Schiff-base/Zn (II) (Fig. 2). Particular vibrational bands of 530 and 590 cm^{-1}, respectively, were observed for the Fe-O bond in the Fe_3O_4 and the Zn-O bond in the Fe_3O_4@SiO_2/Schiff-base/Zn (II) MNC (Fig. 2a and e). In addition, the characteristic Si-O-Si band was observed at approximately 1190 cm^{-1} for the Fe_3O_4@SiO_2 and Fe_3O_4@SiO_2/Schiff-base/Zn (II) (Fig. 2b and e). The stretching band at 1635 ($cm^{[-1}$) (Fig. 2c) was represented by the C = N bond in the Schiff-base ligand. This band emerged at a lower frequency of 1620 cm^{-1} in the Zn (II)/Schiff-base complex (Fig. 2d) and Fe_3O_4@SiO_2/Schiff-base/Zn (II) MNC (Fig. 2e) because of the complex's Zn metal anchoring. The FT-IR evidence has confirmed the synthesis of Fe_3O_4@SiO_2/Schiff-base/Zn (II) MNC based on this finding.

X-Ray diffraction analysis

XRD spectra of (f) Fe_3O_4, (g) Fe_3O_4@SiO_2, (h) Fe_3O_4@SiO_2/Schiff-base/Zn (II), and (i) Schiff-base/Zn (II) are shown in Fig. 2f–i. The six different patterns at $2\theta = 29.89^\circ$, 35.45°, 43.26°, 56.5°, 59.5°, and 66.15°, respectively, reveal the crystallographic spinel structure in the Fe_3O_4 NPs and are correlated with indices 220, 311, 400, 422, 511, and 440 (Fig. 3f)[35]. The previously indicated peaks are also present in the Fe_3O_4@SiO_2 and Fe_3O_4@SiO_2/Schiff-base/Zn (II) at lower intensities (Fig. 3g and h), which show how the Fe_3O_4 NPs were successfully coated with SiO_2 and the Schiff base complex of Zn. Furthermore, Fe_3O_4@SiO_2 exhibits a distinct diffusion peak at $2\theta = 15–25^\circ$, which can be attributed to the coating of Fe_3O_4 MNPs by silica (Fig. 3g)[16]. The Zn (II)/Schiff-base complex attaching to the Fe_3O_4@SiO_2 (Fig. 3h) causes the peak to appear at lower angles. Also, the XRD spectrum of the Schiff-base/Zn (II) complex (Fig. 2i) likely reflects its amorphous or poorly crystalline

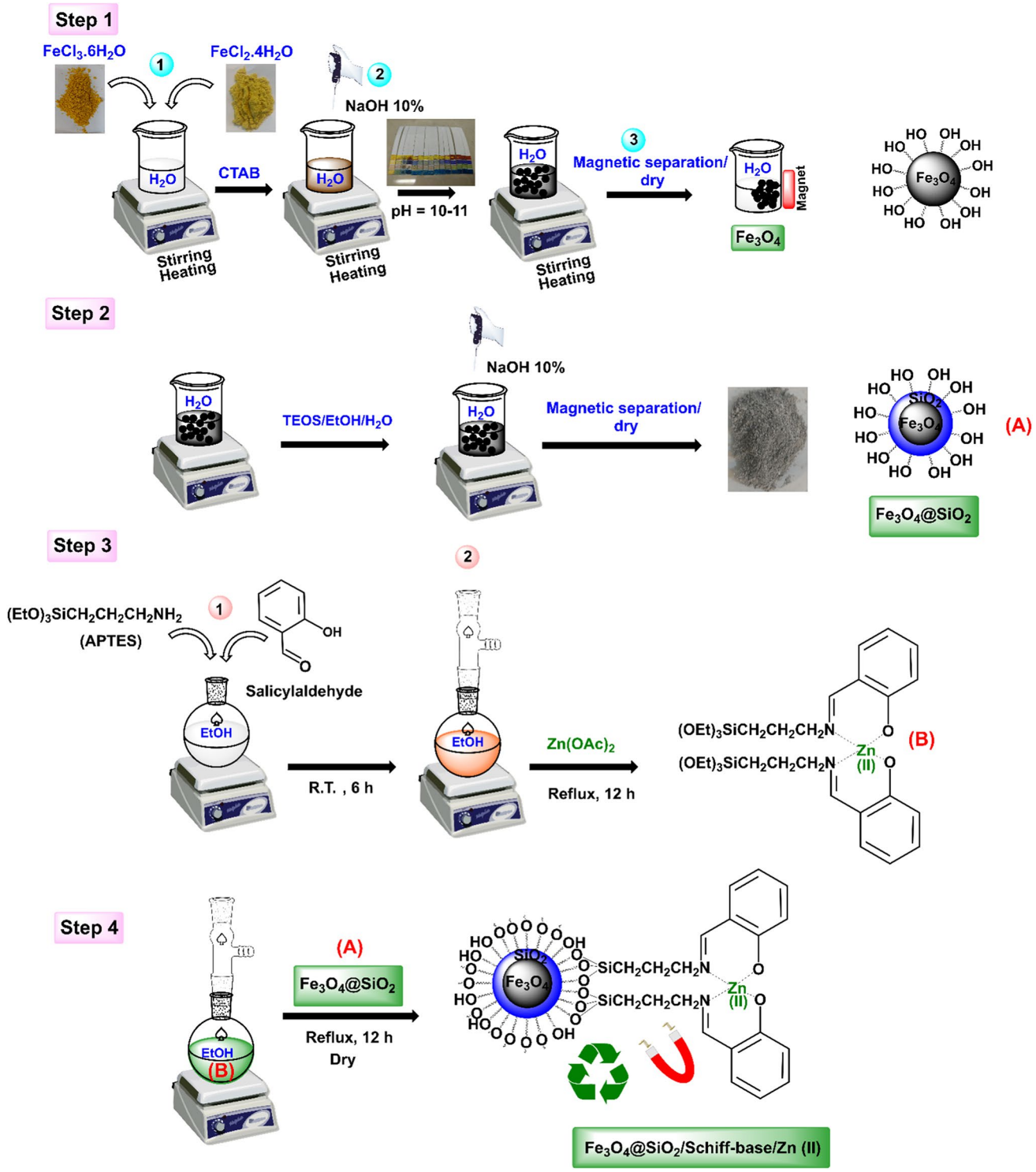

Fig. 1. The preparation process of Fe_3O_4@SiO_2/Schiff-base/Zn (II) MNC.

nature, which is common for such complexes. This is due to the lack of long-range atomic order, flexible ligand structures, and the presence of organic components that contribute to diffuse scattering rather than distinct peaks. Consequently, the Schiff-base/Zn (II) complex does not produce prominent peaks in the XRD spectrum, which aligns with the observed similarity between Fe_3O_4, Fe_3O_4@SiO_2, and Fe_3O_4@SiO_2/Schiff-base/Zn (II). Therefore, the XRD result confirms that the Zn (II)-Schiff base complex is efficiently immobilized on the Fe_3O_4@SiO_2 MNPs without causing any changes to the Fe_3O_4 MNPs' structural integrity.

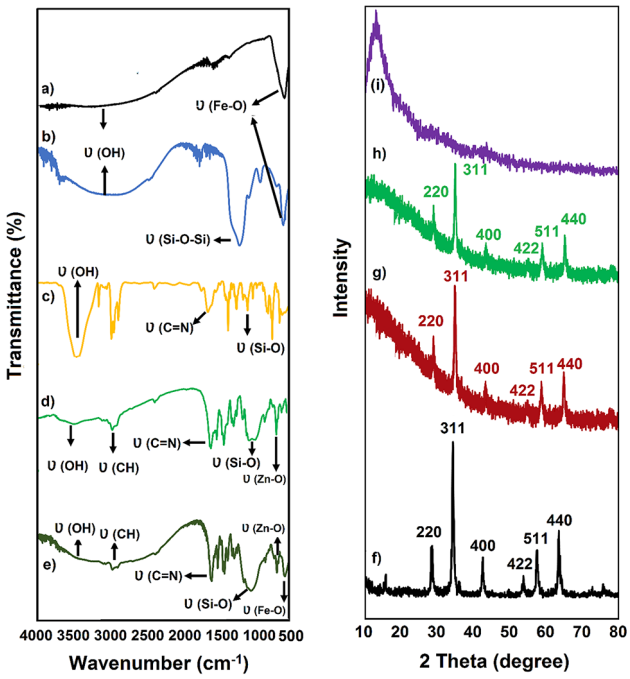

Fig. 2. FT-IR spectra of (**a**) Fe_3O_4, (**b**) Fe_3O_4@SiO_2, (**c**) Schiff-base ligand, (**d**) Schiff-base/Zn (II) and (**e**) Fe_3O_4@SiO_2/Schiff-base/Zn (II); XRD patterns of (**f**) Fe_3O_4, (**g**) Fe_3O_4@SiO_2, (**h**) Fe_3O_4@SiO_2/Schiff-base/Zn (II), and (**i**) Schiff-base/Zn (II).

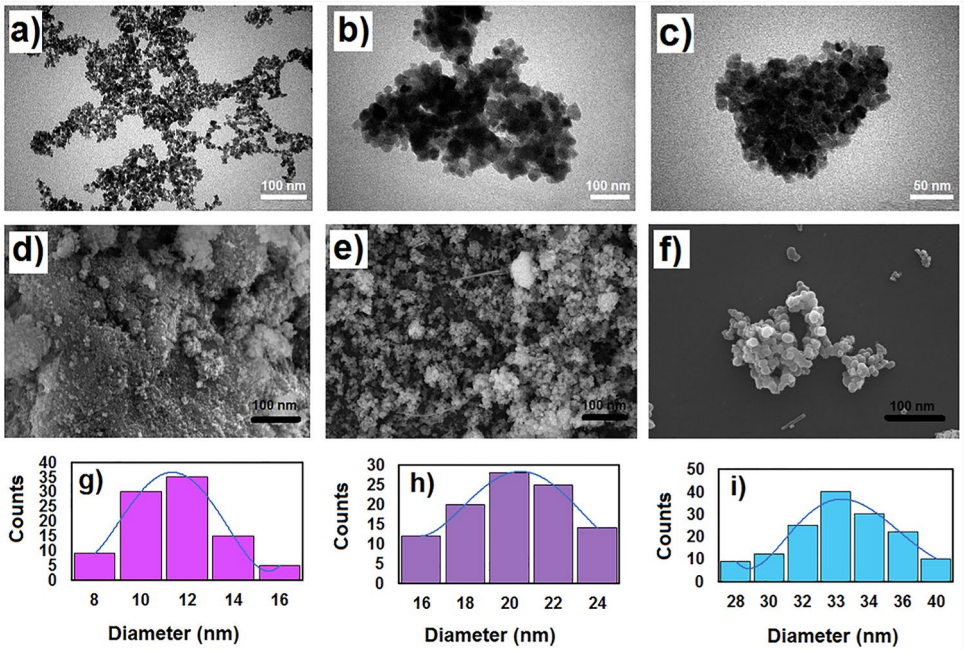

Fig. 3. TEM images of (**a**) Fe_3O_4, (**b**) Fe_3O_4@SiO_2 and (**c**) Fe_3O_4@SiO_2/Schiff-base/Zn (II); SEM images of (**d**) Fe_3O_4, (**e**) Fe_3O_4@SiO_2 and (**f**) Fe_3O_4@SiO_2/Schiff-base/Zn (II); particle size distributions of (**g**) Fe_3O_4, (**h**) Fe_3O_4@SiO_2, and (**i**) Fe_3O_4@SiO_2/Schiff-base/Zn (II).

SEM, TEM, DLS results

Figure 3 shows the TEM, SEM, and DLS results of the Fe_3O_4, Fe_3O_4@SiO_2, and Fe_3O_4@SiO_2/Schiff-base/Zn (II) MNC. Harmonic black spheres with an estimated particle size of 10–15 nm are visible in the Fe_3O_4 TEM picture (Fig. 3a)[35]. Fe_3O_4@SiO_2 MNPs are between 18 and 25 nm in size, as seen in Fig. 3b, and the gray silica layer on their surface preserves the spherical pattern in the TEM image[35]. An average size of 32–40 nm was obtained for

the Fe_3O_4@SiO_2/Schiff-base/Zn (II) MNC (Fig. 3c), and the immobilization of Zn (II)/Schiff-base complex on the Fe_3O_4@SiO_2 NPs did not influence the spherical structural pattern. The NPs (Fig. 3d–f) exhibit homogenous spheres and morphological patterns, demonstrating the successful surface modification of the Fe_3O_4 MNPs with silica layer and the Fe_3O_4@SiO_2 with Zn metal complex subsequently. According to the DLS study, the average size of the Fe_3O_4, Fe_3O_4@SiO_2, and Fe_3O_4@SiO_2/Schiff-base/Zn (II) MNC was 12, 20, and 33 nm, respectively (Fig. 3g-i).

EDX spectrum

The elemental composition of the (a) Fe_3O_4, (b) Fe_3O_4@SiO_2, and (c) Fe_3O_4@SiO_2/Schiff-base/Zn (II) MNC was determined by EDX analysis (Fig. 4). Figure 4a shows the typical elements of Fe and O in Fe_3O_4[35]. The elemental composition spectrum of Fe_3O_4@SiO_2 exhibits a significant amount of Si, indicating that the silica layer has effectively coated the Fe_3O_4 NPs (Fig. 4b)[35]. The elements as O, C, N, Si, and Zn are depicted in Fig. 4c for Schiff-base/Zn (II) complex. The elemental peaks of Fe, O, C, N, Si, and Zn in the Fe_3O_4@SiO_2/Schiff-base/Zn (II) MNC are shown in Fig. 4d. These peaks show that Fe_3O_4@SiO_2 is effectively functionalized with the Zn (II) Schiff-base complex, resulting in the synthesis of Fe_3O_4@SiO_2/Schiff-base/Zn (II) MNC.

VSM and TGA analyses

Using VSM analysis, the superparamagnetic behavior of Fe_3O_4, Fe_3O_4@SiO_2, and Fe_3O_4@SiO_2/Schiff-base/Zn (II) MNC was investigated at ambient temperature. To explore the super-paramagnetization, a magnetic field of up to 8000 Oe at 300 K was used (Fig. 5a-c). No hysteresis phenomena is seen in the magnetization curves, which confirms the magnetization property of the NPs. For Fe_3O_4, Fe_3O_4@SiO_2, and Fe_3O_4@SiO_2/Schiff-base/Zn (II) MNC, the saturation magnetization (Ms) values were determined to be 65.2 (Fig. 5a), 46.1 (Fig. 5b), and 35.5 (Fig. 5c) emu/g, respectively. The modest decrease in Ms values of NPs results from Fe_3O_4 being functionalized with SiO_2 core-shell and then Zn (II)/Schiff-base complex. However, it has no noticeable effect on the magnetization properties of NPs, particularly Fe_3O_4@SiO_2/Schiff-base/Zn (II) MNC. By assessing the magnetization of NPs in the presence of an external magnetic field, this evidence is ultimately validated (Fig. 5d). It would be easy and quick to separate the Fe_3O_4@SiO_2/Schiff-base/Zn (II) MNC, which is crucial for recovering process.

Fe_3O_4, Fe_3O_4@SiO_2, and Fe_3O_4@SiO_2/Schiff-base/Zn (II) MNC were tested with TGA analysis for thermal stability in the temperature range of 25 to 750 ˚C (Fig. 5e-g). By raising the temperature, the thermograms display the percentage of volatile components. At higher temperatures, the thermally stable structure of the NPs

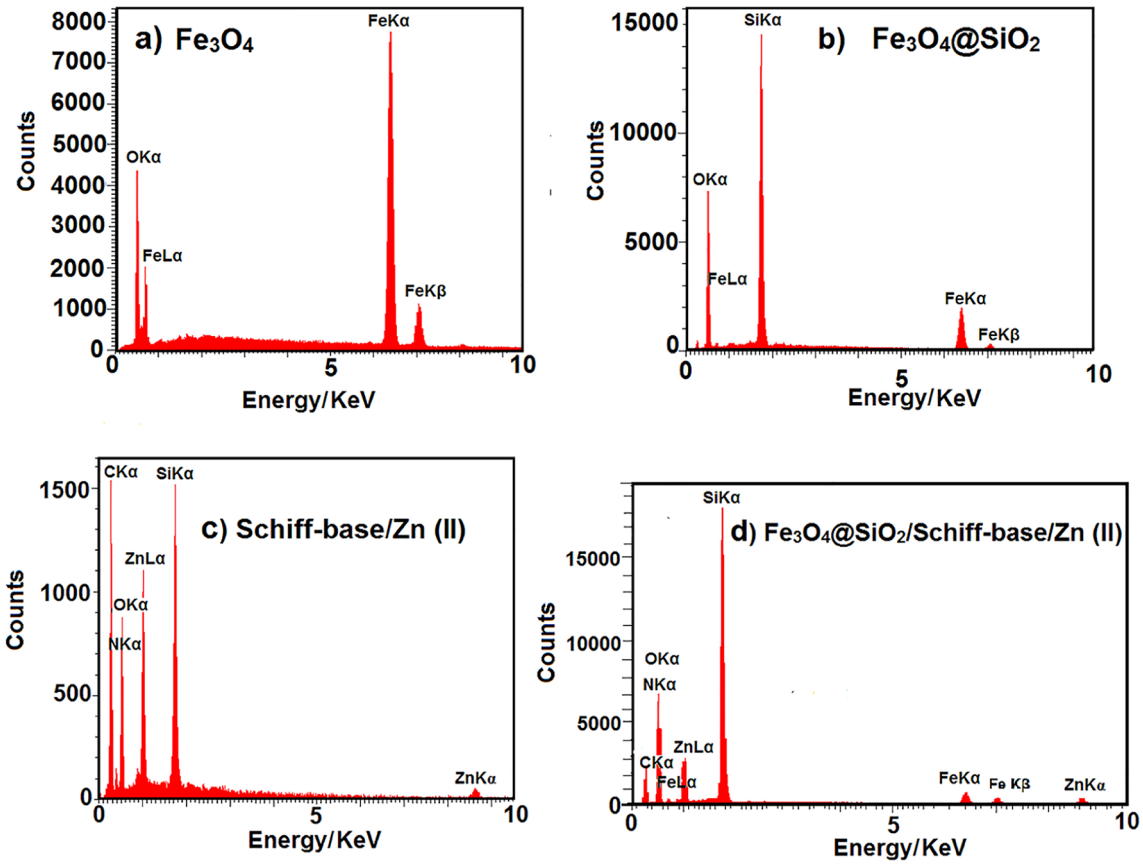

Fig. 4. EDX spectra of (**a**) Fe_3O_4, (**b**) Fe_3O_4@SiO_2, (**c**) Schiff-base/Zn (II) and (**d**) Fe_3O_4@SiO_2/Schiff-base/Zn (II) MNC.

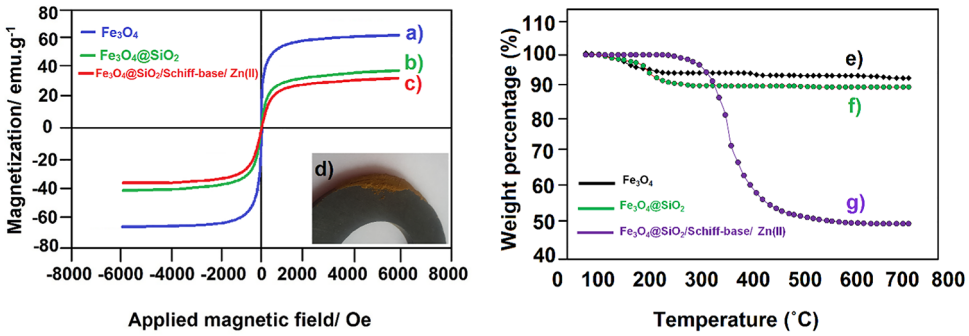

Fig. 5. Magnetization curves of (**a**) Fe_3O_4, (**b**) Fe_3O_4@SiO_2, and (**c**) Fe_3O_4@SiO_2/Schiff-base/Zn (II), (**d**) magnetic characteristic image of Fe_3O_4@SiO_2/Schiff-base/Zn (II); TGA spectra of (**e**) Fe_3O_4, (**f**) Fe_3O_4@SiO_2 and (**g**) Fe_3O_4@SiO_2/Schiff-base/Zn (II) MNC.

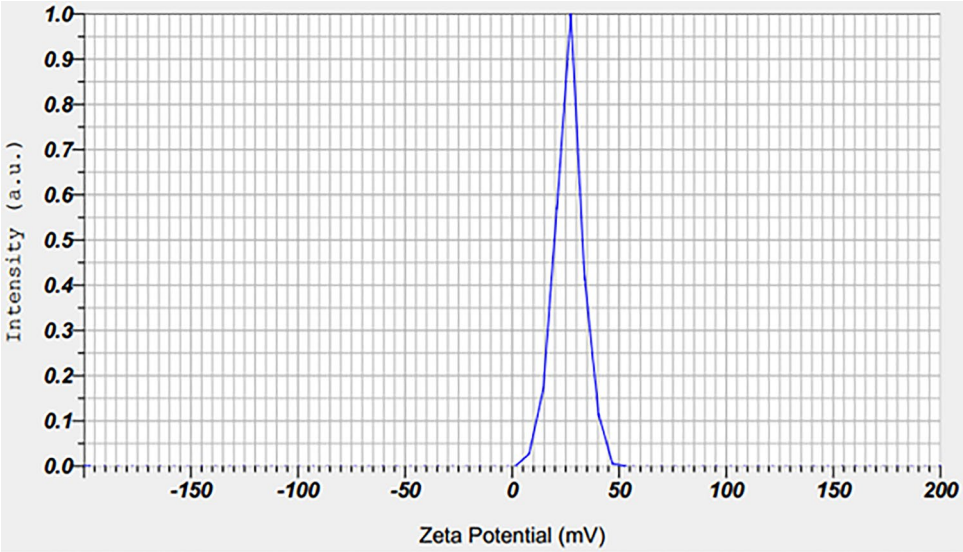

Fig. 6. Zeta potential of Fe_3O_4@SiO_2/Schiff-base/Zn (II) MNC.

is revealed, despite negligible mass loss in the Fe_3O_4 and Fe_3O_4@SiO_2 slopes (Fig. 5e and f). The modest decrease can be attributed to the elimination of adsorbed water, intact organic solvents, and hydroxyl groups between 100 and 500 ˚C. In the Fe_3O_4@SiO_2/Schiff-base/Zn (II) MNC, the slope also decreases up to 300–370 ˚C, at which point the mass loss is ascribed to the decomposition of organic components (Fig. 5g). This observation confirms the outstanding thermal resilience of the Fe_3O_4@SiO_2/Schiff-base/Zn (II) MNC at high temperatures, as well as the successful immobilization of Zn (II)/Schiff-base complex on the Fe_3O_4@SiO_2 MNPs.

Zeta potential of Fe_3O_4@SiO_2/Schiff-base/Zn (II)

According to Fig. 6, a zeta potential of + 26.5 mV indicates that Fe_3O_4@SiO_2/Schiff-base/Zn (II) MNC possess a moderate positive surface charge, which is highly beneficial for antimicrobial activities. This positive charge facilitates strong interactions with negatively charged microbial cell membranes, leading to effective antibacterial and antifungal actions through membrane disruption, ROS generation, and interference with essential cellular processes. Additionally, the multifunctional design of your NPs enhances their stability, targeting capabilities, and overall antimicrobial efficacy.

Antifungal activity of Fe_3O_4@SiO_2/Schiff-base/Zn (II) by broth microdilution method

Table 1 displays the MIC and MFC values of Fe_3O_4@SiO_2/Schiff-base/Zn (II) MNC against fungal species investigated in this study. We examined the antifungal efficacy of Fe_3O_4@SiO_2/Schiff-base/Zn (II) against six *Candida* species. Fe_3O_4@SiO_2/Schiff-base/Zn (II) MNC demonstrated effective inhibition of growth for all tested yeast strains at concentrations ranging from 8 to 64 µg/mL. It is noteworthy that these *Candida* species are commonly associated with candidemia, and their resistance to antifungal agents, such as fluconazole, poses considerable challenges for effective treatment. These infections can manifest in various clinical scenarios and are easily transmitted in healthcare settings, contributing to nosocomial infections[40]. Consequently, the observed results highlight the potential efficacy of Fe_3O_4@SiO_2/Schiff-base/Zn (II) MNC against this pathogen, offering

Fungi Standard strains	Organisms	ATCC/CBS	Fe_3O_4@SiO_2/Schiff-base/Zn (II)			Control (Fluconazole)
			MIC90 (µg/mL)	MFC (µg/mL)	ZOI[a] (mm)	
Fungi species	*C. albicans*	C (562)	32	64	15	8
	C. glabrata	A (90030)	64	128	10	4
	C. dubliniensis	C (8501)	32	32	14	2
	C. krusei	A (6258)	16	32	12	8
	C. tropicalis	A (750)	8	16	11	16
	C. parapsilosis	A (4344)	16	32	15	4

Table 1. Antifungal effects of Fe_3O_4@SiO_2/Schiff-base/Zn (II) on the fungi strains based on broth microdilution method. [a]ZOI: Zone of inhibition by disc diffusion method.

promise in addressing these significant challenges. Furthermore, in the case of *C. albicans*, the most prevalent fungus responsible for a wide range of infections, from mild skin and mucosal conditions to severe invasive diseases[41], this MNC formulation demonstrated considerable antifungal activity.

The antifungal activity of Fe_3O_4@SiO_2/Schiff-base/Zn (II) against *Candida* species can be attributed to several factors. Zn is an essential trace element for many living organisms, including fungi. When in NPs form, zinc can be taken up by fungal cells, disrupting their normal metabolic processes[40]. Zn NPs can generate reactive oxygen species (ROS) such as superoxide radicals and hydrogen peroxide (Fig. 7a). These ROS can cause oxidative stress and damage to fungal cell membranes, proteins, and DNA, leading to cell death (Fig. 7a). On the other hand, Zn NPs can interact with fungal cell membranes, causing structural damage and compromising the integrity of the membrane. This disruption can lead to the leakage of cellular contents and ultimately cell death (Fig. 7a)[42]. These NPs can inhibit the activity of certain enzymes that are crucial for fungal growth and metabolism. This disruption of enzyme function can interfere with essential fungal processes, impairing their ability to thrive. It is important to note that while Zn nanoparticles (NPs) have shown antifungal properties in laboratory studies, their practical application in antifungal treatments may require further research and development[43]. The effectiveness of Zn NPs as antifungal agents can also be influenced by factors such as the type of fungus, the size and surface properties of the NPs, and the specific conditions under which they are applied. Furthermore, safety considerations and potential environmental impacts must be carefully evaluated when using NPs for antifungal purposes[44].

Antibacterial activity of Fe_3O_4@SiO_2/Schiff-base/Zn (II) by broth microdilution method

According to the results of the MIC shown in Table 2, Fe_3O_4@SiO_2@Schiff-base/Zn (II) was found to exhibit an antimicrobial action against bacteria such as *S. aureus*, *E. coli*, *P. aeruginosa*, and *E. faecalis*, commonly present in infections. The antibacterial activity of Fe_3O_4@SiO_2/Schiff-base/Zn (II) is primarily attributed to its ability to disrupt bacterial cell structures and generate reactive oxygen species (ROS) (Fig. 7b). The presence of Zn is significantly vital in the interpretation of its biological functions. The presence of the Schiff-base ligand enhances the interaction of the Zn with bacterial membranes, leading to increased permeability and ultimately cell lysis (Fig. 7b)[45]. This mechanism involves the chelation of metal ions, which can interfere with essential bacterial enzymes and metabolic processes. Additionally, the Zn component contributes to the generation of ROS, which further damage cellular components, including lipids, proteins, and nucleic acids, thereby promoting bacterial cell death (Fig. 7b)[46]. The combined effects of structural disruption and oxidative stress make Fe_3O_4@SiO_2/Schiff-base/Zn (II) a potent antibacterial agent against various pathogens.

Antimicrobial activity by disk diffusion method

Figure 8 depicts the antimicrobial activity of Fe_3O_4@SiO_2@Schiff-base/Zn (II) against *Escherichia coli*, *Staphylococcus aureus*, *Pseudomonas aeruginosa*, and *Candida albicans* using the disc diffusion method. The ZOI of each pathogen was measured and reported in Tables 1 and 2.

The incorporation of magnetic properties into Schiff-base/Zn (II) complexes has not been widely explored, particularly in the context of antimicrobial applications. Our results demonstrate that the addition of magnetic functionality enhances the therapeutic potential of the complex, allowing for targeted delivery to infection sites, a crucial advancement over traditional antimicrobial agents. Moreover, the ability to magnetically control the release of the antimicrobial agent could significantly improve the treatment efficacy while minimizing side effects. This dual functionality represents a novel approach that combines the antimicrobial potency of Schiff-base/Zn (II) complexes with the benefits of magnetic targeting, a concept that could be applied in future drug delivery systems.

Biofilm formation inhibition

The formation of *C. albicans* biofilm in the presence of Fe_3O_4@SiO_2/Schiff-base/Zn (II) at concentrations ranging from 0.12 to 64 µg/mL was quantitatively measured using the XTT reduction assay (Table 3; Fig. 9). As shown, biofilm formation was inhibited by Fe_3O_4@SiO_2/Schiff-base/Zn (II) by up to 76% after 48 h. This formulation demonstrated significant activity in inhibiting biofilm formation, as evidenced by a lower absorbance reading compared to the untreated control (Fig. 9). The study on biofilm formation inhibition by Fe_3O_4@SiO_2/Schiff-base/Zn (II) MNC presents promising results in combating *C. albicans*, a common fungal pathogen responsible for various infections. It has been reported that metal complexes, in general, disrupt pre-formed biofilms by

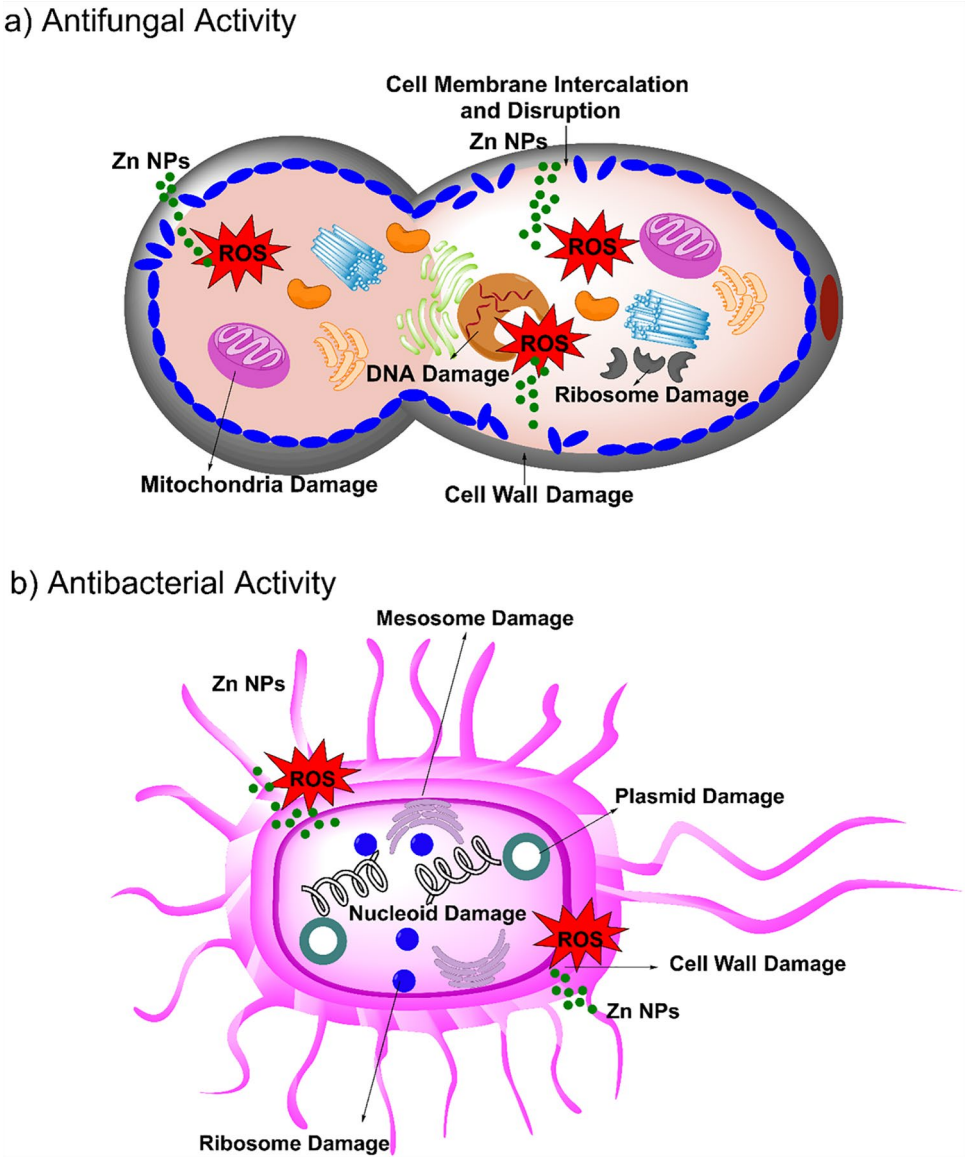

Fig. 7. Plausible mechanism of action of Fe_3O_4@SiO_2@Schiff-base/Zn (II) MNC as an (**a**) antifungal and (**b**) antibacterial agent.

Strains	Organisms	ATCC	Fe_3O_4@SiO_2/Schiff-base/Zn (II)			Control (cotrimoxazole)
			MIC (µg/mL)	MBC (µg/mL)	ZOI[a] (mm)	
Bacteria Standard	*S. aureus*	52,268	128	256	12	4
	E. coli	25,922	256	256	16	32
	P. aeruginosa	27,853	512	Growth	15	64
	E. faecalis	11,700	64	128	10	16

Table 2. Antibacterial effects of Fe_3O_4@SiO_2@Schiff-base/Zn (II) against different bacteria strains based on the broth microdilution method. [a]ZOI: Zone of inhibition by disc diffusion method.

destabilizing the extracellular matrix, which is essential for biofilm integrity. This destabilization may provoke the detachment of cells from the biofilm structure, making them more susceptible to antifungal agents. Given that Fe_3O_4@SiO_2/Schiff-base/Zn (II) effectively inhibits biofilm formation, it is plausible that this complex interferes with quorum-sensing mechanisms that regulate biofilm development.

The ability of this nanocomposite to achieve 76% biofilm inhibition is attributed to its dual mechanisms: the disruption of extracellular matrix stability and interference with quorum sensing pathways. This dual-action

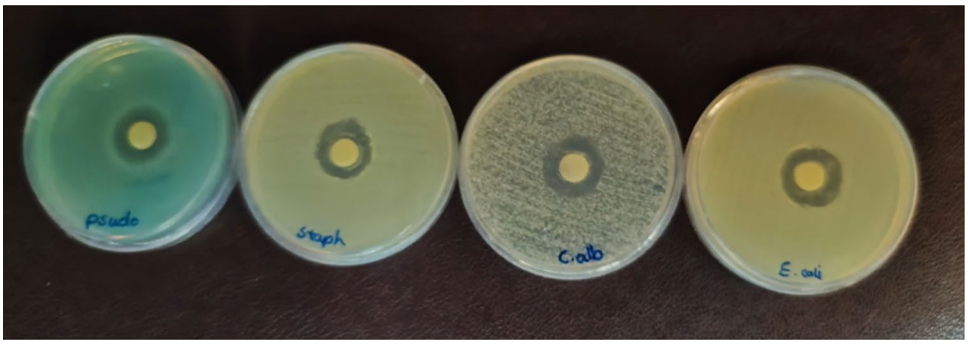

Fig. 8. Antimicrobial activities of Fe_3O_4@SiO_2@Schiff-base/Zn (II) on the yeast fungi and bacteria standard strains based on the disk diffusion method.

Fe_3O_4@SiO_2/Schiff-base/Zn (II) Concentration (µg/mL)	Optical Density ± SD	Biofilm Inhibition (%)
0.12	0.63 ± 0.001	12.2
0.25	0.49 ± 0.002	30.7
0.5	0.48 ± 0.03	31.0
1	0.42 ± 0.002	40.1
2	0.4 ± 0.001	43.1
4	0.39 ± 0.008	55.7
8	0.31 ± 0.001	60.3
16	0.29 ± 0.002	62.3
32	0.21 ± 0.001	73.5
64	0.184 ± 0.002	76.5

Table 3. Formation of *C. Albicans* biofilm in the presence of Fe_3O_4@SiO_2/Schiff-base/Zn (II) by XTT reduction assay.

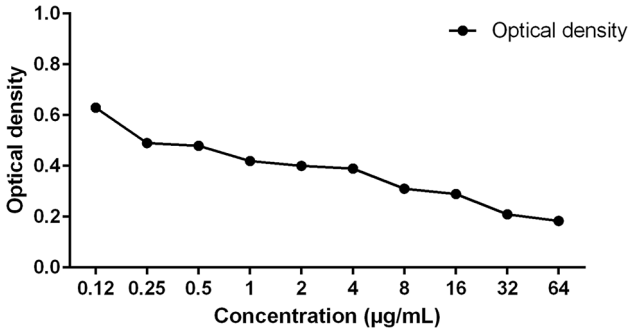

Fig. 9. Inhibition of *Candida* biofilm formation in different concentrations of Fe_3O_4@SiO_2/Schiff-base/Zn (II).

strategy has rarely been reported for nanoparticle-based systems, establishing this material as a frontrunner in biofilm-targeted therapies. The findings from this study provide a significant leap forward in the design of antimicrobial agents. By combining targeted antimicrobial activity with biofilm inhibition and magnetic recoverability, this work sets the stage for developing advanced materials capable of addressing clinical and environmental challenges posed by multidrug-resistant microorganisms.

Cell viability and proliferation assessment

An MTT assay was carried out to further explore the L929 cell proliferation with Fe_3O_4@SiO_2/Schiff-base/Zn (II) MNC on days 1, 3, and 5. As depicted in Fig. 10, the concentrations of 64, 128, and 256 µg/mL of the Zn NPs were treated. All data on each day, except for 256 µg/mL on the 5th day, indicated no significant difference during the test, which revealed that almost all the concentrations were biocompatible in comparison with the control group. It seems that over time, the concentration of 256 µg/mL of Zn was cytotoxic.

The stability of Fe_3O_4@SiO_2/Schiff-base/Zn (II) MNC was assessed after 3 months (Fig. 11). The UV-Vis spectrum depicts a broad peak which illustrate the maintanance of the tetrahedral geometry of Zn in the MNC

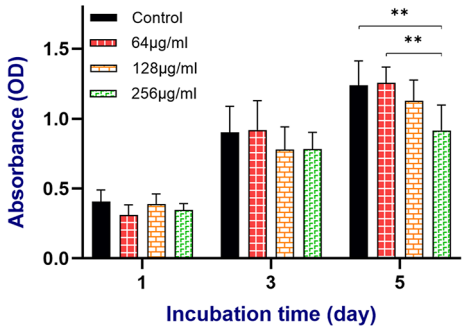

Fig. 10. Cell viability (MTT assay): The proliferation of control and different concentrations of samples during the incubation times of the first, third, and fifth day.

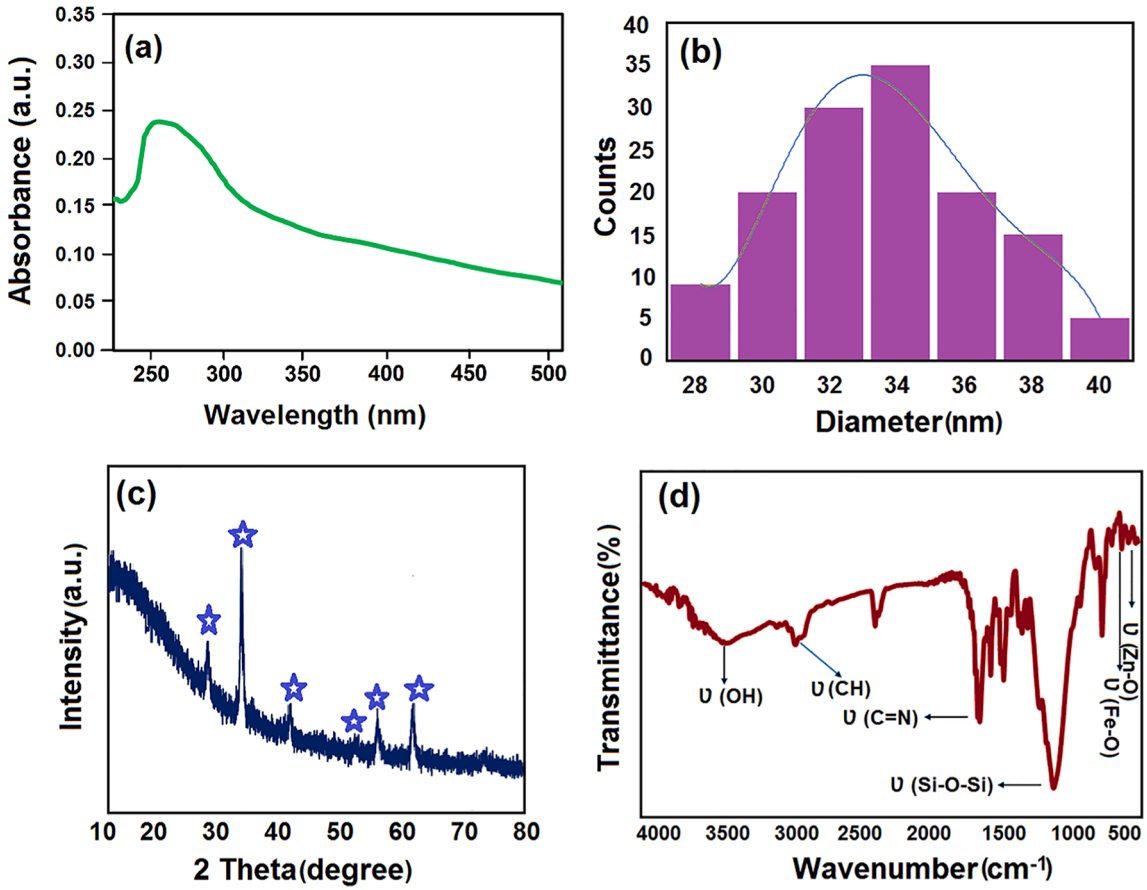

Fig. 11. The stability of Fe_3O_4@SiO_2/Schiff-base/Zn (II) MNC after 3 months was evaluated by (**a**) UV, (**b**) DLS, (**c**) XRD, and (**d**) FT-IR.

structure (Fig. 11a). The size distribution of Fe_3O_4@SiO_2/Schiff-base/Zn (II) MNC reveals that the nano-size property was not altered, which demonstrates the stability of the MNC (Fig. 11b). The XRD pattern of the Fe_3O_4@SiO_2/Schiff-base/Zn (II) MNC is similar to that in the fresh MNC (Fig. 2h), indicating the stable crystallographic spinel structure of Fe_3O_4 NPs (Fig. 11c). The similarity of Fe_3O_4@SiO_2/Schiff-base/Zn (II) MNC both in fresh FT-IR (Fig. 2e) and 3-month one (Fig. 11d) is an evidence for stability of the MNC.

Conclusion

In this study, we successfully synthesized and characterized Fe_3O_4@SiO_2/Schiff-base/Zn (II) MNC using a coprecipitation method followed by silica coating and Schiff-base complexation. The successful synthesis was confirmed through various characterization techniques, including FT-IR, XRD, SEM, TEM, EDX, VSM, and TGA, which demonstrated the formation of a well-defined core-shell structure and the effective immobilization

of the Schiff-base ligand and Zn (II) ions. The synthesized MNC exhibited significant antifungal and antibacterial activity against various microbial strains, indicating their potential as effective antimicrobial agents. The antimicrobial and antibiofilm activites of the Fe_3O_4@SiO_2/Schiff-base/Zn (II) MNC, which could be beneficial in clinical applications, particularly in treating infections caused by resistant strains. Furthermore, the cytotoxicity assessment using the MTT assay confirmed the biocompatibility of the MNC, which is crucial for their future therapeutic applications. Overall, the findings highlight the potential of Fe_3O_4@SiO_2/Schiff-base/Zn (II) MNC in medical and environmental applications, paving the way for further studies on their efficacy and safety in vivo.

Data availability

All data generated or analyzed during this study are included in this published article.

Received: 9 November 2024; Accepted: 13 January 2025
Published online: 17 February 2025

References

1. Laxminarayan, R. et al. -Hara Gl Fau -, So Ad Fau - Bigdeli, Peralta Aq Fau - Qamar, - Wright Gd Fau - Brown, E. D., Brown Ed Fau - Cars, O. & Cars, O. Antibiotic resistance-the need for global solutions. *Lancet. Infect. Dis.* 13, 1057–1098. (2013). https://doi.org/10.1016/S1473-3099(13)70318-9
2. Dolecek, C., Shakoor, S., Basnyat, B., Okwor, T. & Sartorius, B. Drug-resistant bacterial infections: We need urgent action and investment that focus on the weakest link. *PLoS Biol.* **20**, e3001903. https://doi.org/10.1371/journal.pbio.3001903 (2022).
3. Karam, G., Chastre, J., Wilcox, M. H. & Vincent, J. L. Antibiotic strategies in the era of multidrug resistance. *Crit. Care*. **20**, 136. https://doi.org/10.1186/s13054-016-1320-7 (2016).
4. Baran, A., Kwiatkowska, A. & Potocki, L. Antibiotics and bacterial resistance-A short story of an endless arms race. *Int. J. Mol. Sci.* **24**, 5777. https://doi.org/10.3390/ijms24065777 (2023).
5. Husna, A. et al. Extended-spectrum β-Lactamases (ESBL): Challenges and opportunities. *Biomedicines* **11**, 2937. https://doi.org/10.3390/biomedicines11112937 (2023).
6. Donkor Eric, S. & Codjoe Francis, S. Methicillin resistant and extended spectrum beta-lactamase producing: A therapeutic challenge in the 21 century. *Open. J. Med. Microbiol.* **13**, 94–100. https://doi.org/10.2174/1874285801913010094 (2019).
7. Dolande, M. et al. Candida Auris: Antifungal multi-resistant emerging yeast. *Curr. Fungal Infect. Rep.* **11**, 197–202. https://doi.org/10.1007/s12281-017-0299-0 (2017).
8. Amaro, F., Morón, Á., Díaz, S., Martín-González, A. & Gutiérrez, J. C. Metallic nanoparticles—friends or foes in the battle against antibiotic-resistant bacteria. *Microorganisms* **9**, 364. https://doi.org/10.3390/microorganisms9020364 (2021).
9. Kalakonda, P. et al. Comparison of multi-metallic nanoparticles-alternative antibacterial agent: Understanding the role of their antibacterial properties. *J. Inorg. Organomet. Polym. Mater.* **34**, 2203–2218. https://doi.org/10.1007/s10904-023-02960-x (2024).
10. Gautam, S. et al. Transition metal-based nanoparticles as potential antimicrobial agents: Recent advancements, mechanistic, challenges, and future prospects. *Discover Nano*. **18**, 84. https://doi.org/10.1186/s11671-023-03861-1 (2023).
11. Chakraborty, N. et al. Nanobiotics against antimicrobial resistance: Harnessing the power of nanoscale materials and technologies. *J. Nanobiotechnol.* **20**, 375. https://doi.org/10.1186/s12951-022-01573-9 (2022).
12. Abbasi, R., Shineh, G., Mobaraki, M., Doughty, S. & Tayebi, L. Structural parameters of nanoparticles affecting their toxicity for biomedical applications: A review. *J. Nanoparticle Res.* **25**, 43. https://doi.org/10.1007/s11051-023-05690-w (2023).
13. Nguyen, M. D., Tran, H. V., Xu, S. & Lee, T. R. Fe_3O_4 nanoparticles: Structures, synthesis, magnetic properties, surface functionalization, and emerging applications. *Appl. Sci.* **11**, 11301. https://doi.org/10.3390/app112311301 (2021).
14. Bakhtari, A. et al. Effects of Dextran-Coated Superparamagnetic Iron Oxide nanoparticles on mouse embryo development, antioxidant enzymes and apoptosis genes expression, and ultrastructure of sperm, oocytes and Granulosa cells. *Int. J. Fertil. Steril.* **14**, 161–170. https://doi.org/10.22074/ijfs.2020.6167 (2020).
15. Hassanloie, N. et al. Preparation of Fe_3O_4@SiO_2@Cu-MoO_3 core–shell nanostructures: Synergistics effects of copper and molybdenum for catalytic enhancement. *J. Porous Mater.* **30**, 859–869. https://doi.org/10.1007/s10934-022-01379-y (2023).
16. Azadi, S., Sardarian, A. R. & Esmaeilpour, M. Nano Cr(III) Schiff-base complex supported on magnetic Fe_3O_4@SiO_2: Efficient, heterogeneous, and recoverable nanocatalyst for chemoselective synthesis of 1,2-disubstituted benzimidazoles. *Monatsh Chem.* **154**, 887–903. https://doi.org/10.1007/s00706-023-03100-4 (2023).
17. Ceramella, J. et al. A review on the antimicrobial activity of Schiff bases: Data collection and recent studies. *Antibiotics* **11**, 191. https://doi.org/10.3390%2Fantibiotics11020191 (2022).
18. Aljahdali, M. S. & El-Sherif, A. A. Synthesis and biological evaluation of novel Zn(II) and Cd(II) Schiff base complexes as antimicrobial, antifungal, and antioxidant agents. *Bioinorg. Chem. Appl.* 8866382. (2020). https://doi.org/10.1155/2020/8866382 (2020).
19. Abdel-Rahman, L. H., Abu-Dief, A. M., El-Khatib, R. M. & Abdel-Fatah, S. M. Some new nano-sized Fe(II), cd(II) and zn(II) Schiff base complexes as precursor for metal oxides: Sonochemical synthesis, characterization, DNA interaction, in vitro antimicrobial and anticancer activities. *Bioorg. Chem.* **69**, 140–152. https://doi.org/10.1016/j.bioorg.2016.10.009 (2016).
20. Kumar, S. et al. Co(II), ni(II), Cu(II) and zn(II) complexes of Schiff base ligands: Synthesis, characterization, DFT, in vitro antimicrobial activity and molecular docking studies. *Res. Chem. Intermed.* **49**, 939–965. https://doi.org/10.1007/s11164-022-04941-0 (2022).
21. Eshaghi Malekshah, R., Fahimirad, B., Khaleghian, A., Synthesis, Characterization, B. & Application molecular dynamic simulation and molecular docking of Schiff base complex of Cu(II) supported on Fe_3O_4/SiO_2/APTS. *Int. J. Nanomed.* **20**, 2583–2603. https://doi.org/10.2147/ijn.s231062 (2020).
22. Nazirkar, B., Mandewale, M. & Yamgar, R. Synthesis, characterization and antibacterial activity of Cu (II) and zn (II) complexes of 5-aminobenzofuran-2-carboxylate Schiff base ligands. *J. Taibah Univ. Sci.* **13**, 440–449. https://doi.org/10.1080/16583655.2019.1592316 (2019).
23. Chaabane, L. et al. Synthesis and characterization of Ni (II), Cu (II), Fe (II) and Fe_3O_4 nanoparticle complexes with tetraaza macrocyclic Schiff base ligand for antimicrobial activity and cytotoxic activity against cancer and normal cells. *Appl. Organomet. Chem.* **33**, e4860. https://doi.org/10.1002/aoc.4860 (2019).
24. Althobiti, H. A. & Zabin, S. A. New Schiff bases of 2-(quinolin-8-yloxy)acetohydrazide and their Cu(II), and zn(II) metal complexes: Their in vitro antimicrobial potentials and in silico physicochemical and pharmacokinetics properties. *Open. Chem.* **18**, 591–607. https://doi.org/10.1515/chem-2020-0085 (2020).
25. Kargar, H., adabi ardakani, A., Tahir, M., Ashfaq, M. & Munawar, K. S. Synthesis, spectral characterization, crystal structure and antibacterial activity of nickel(II), copper(II) and zinc(II) complexes containing ONNO donor Schiff base ligands. *J. Mol. Struct.* **1233**, 130112. https://doi.org/10.1016/j.molstruc.2021.130112 (2021).
26. Al-Shboul, T. M. A. et al. Characterization, computational and biological activity of some Schiff bases and their Fe, Cu and Zn complexes. *Inorganics* **10**, 112. https://doi.org/10.3390/inorganics10080112 (2022).

27. Elkanzi, N. A. A. et al. Synthesis, physicochemical properties, biological, molecular docking and DFT investigation of Fe(III), Co(II), ni(II), Cu(II) and zn(II) complexes of the 4-[(5-oxo-4,5-dihydro-1,3-thiazol-2-yl)hydrazono]methyl}phenyl 4-methylbenzenesulfonate Schiff-base ligand. *Polyhedron* **230**, 116219. https://doi.org/10.1016/j.poly.2022.116219 (2023).
28. Dinku, D. et al. Antimicrobial activities and docking studies of new Schiff base ligand and its Cu(II), zn(II) and ni (II) complexes: Synthesis and characterization. *Inorg. Chem. Commun.* **160**, 111903. https://doi.org/10.1016/j.inoche.2023.111903 (2024).
29. Sevgi, F., Bagkesici, U., Kursunlu, A. N. & Guler, E. Fe (III), Co(II), ni(II), Cu(II) and zn(II) complexes of schiff bases based-on glycine and phenylalanine: synthesis, magnetic/thermal properties and antimicrobial activity. *J. Mol. Struct.* **1154**, 256–260. https://doi.org/10.1016/j.molstruc.2017.10.052 (2018).
30. Al-Qadsy, I. et al. Antimicrobial activity of Novel Ni(II) and zn(II) complexes with (E)-2-((5-Bromothiazol-2-yl)imino)methyl) phenol ligand: Synthesis, characterization and molecular Docking studies. *Antibiotics* **12**, 1634. https://doi.org/10.3390/antibiotics12111634 (2023).
31. Zaltariov, M. F. et al. Synthesis, characterization and antimicrobial activity of new Cu(II) and zn(II) complexes with Schiff bases derived from trimethylsilyl-propyl-p-aminobenzoate. *Polyhedron* **100**, 121–131. https://doi.org/10.1016/j.poly.2015.07.030 (2015).
32. Amri, N. & Alaghaz, A. N. M. A. Synthesis, structural investigations, in vitro cytotoxicity, apoptotic activity, cell cycle analysis, and molecular modeling studies of nano-sized zn(II) Schiff base complex. *Appl. Organomet. Chem.* **38**, e7577. https://doi.org/10.1002/aoc.7577 (2024).
33. Panahandehjo, S., Lashanizadegan, M., Mohammadi, K. & Yazdian, F. Synthesis and characterization of N4-donor Schiff base copper(II) immobilized on superparamagnetic Fe_3O_4@SiO_2 and its use as a recyclable catalyst for oxidation of alkenes, alcohols, and determination of antibacterial activity. *Inorg. Nano-Met Chem.* 1–11. https://doi.org/10.1080/24701556.2023.2240769 (2023).
34. Poor Heravi, M. R., Mahjouri, D., Vessally, E. & Mohammadi, B. High Catalytic activity, recyclable and magnetically separable Nanocatalyst Fe_3O_4@SiO_2-Schiff base-Pd(II) for synthesis of 12H-Benzo[5,6]Chromeno[2,3-b]pyridine-10-Carbonitriles and evaluation of antibacterial activity. *Polycycl. Aromat. Comp.* **44**, 2924–2941. https://doi.org/10.1080/10406638.2023.2225681 (2024).
35. Azadi, S. et al. Antifungal activity of Fe_3O_4@SiO_2/Schiff-base/Cu(II) magnetic nanoparticles against pathogenic Candida species. *Sci. Rep.* **14**, 5855–5865. https://doi.org/10.1038/s41598-024-56512-5 (2024).
36. Esmaeilpour, M., Sardarian, A. R. & Javidi, J. Schiff base complex of metal ions supported on superparamagnetic Fe_3O_4@SiO_2 nanoparticles: an efficient, selective and recyclable catalyst for synthesis of 1,1-diacetates from aldehydes under solvent-free conditions. *Appl. Catal. Gen.* **445–446**, 359–367. https://doi.org/10.1016/j.apcata.2012.09.010 (2012).
37. Torabiardekani, N. et al. Encapsulation of Zataria multiflora essential oil in polyvinyl alcohol/chitosan/gelatin thermo-responsive hydrogel: synthesis, physico-chemical properties, and biological investigations. *Int. J. Biol. Macromol.* **243**, 125073. https://doi.org/10.1016/j.ijbiomac.2023.125073 (2023).
38. Hashempur, M. H. et al. Enrichment of creatine-gelatin cryogel with Zataria multiflora essential oil and titanium dioxide nanoparticles as a potential wound dressing. *Mater. Today Chem.* **38**, 102069. https://doi.org/10.1016/j.mtchem.2024.102069 (2024).
39. Karami, F. et al. Chitosan-based emulgel and xerogel film containing Thymus pubescens essential oil as a potential wound dressing. *Carbohydr. Polym.* **318**, 121156. https://doi.org/10.1016/j.carbpol.2023.121156 (2023).
40. Zareshahrabadi, Z. et al. Magnetic chitosan nanoparticles loaded with amphotericin B: Synthesis, properties and potentiation of antifungal activity against common human pathogenic fungal strains. *Int. J. Biol. Macromol.* **222**, 1619–1631. https://doi.org/10.1016/j.ijbiomac.2022.09.244 (2022).
41. Moshaverinia, M., Sahmeddini, S., Lavee, F., Zareshahrabadi, Z. & Zomorodian, K. Antimicrobial and anti-biofilm activities of Thymus fallax essential oil against oral pathogens. *Biomed. Res. Int.* **2022** (9744153). https://doi.org/10.1155/2022/9744153 (2022).
42. Sadeghian, S. et al. Imidazole derivatives as novel and potent antifungal agents: Synthesis, biological evaluation, molecular docking study, molecular dynamic simulation and ADME prediction. *J. Mol. Struct.* **1302**, 137447. https://doi.org/10.1016/j.molstruc.2023.137447 (2024).
43. Mohd Yusof, H., Mohamad, R., Zaidan, U. H. & Abdul Rahman, N. A. Microbial synthesis of zinc oxide nanoparticles and their potential application as an antimicrobial agent and a feed supplement in animal industry: A review. *J. Anim. Sci. Biotechnol.* **10**, 57. https://doi.org/10.1186/s40104-019-0368-z (2019).
44. Xie, J. et al. Recent advances in ZnO nanomaterial-mediated Biological Applications and Action mechanisms. *Nanomater* **13**, 1500. https://doi.org/10.3390/nano13091500 (2023).
45. Brayner, R. et al. Benedetti Mf Fau - Fiévet, F. Toxicological impact studies based on Escherichia coli bacteria in ultrafine ZnO nanoparticles colloidal medium. *Nano Lett.* 6, 866–870 (2006). https://doi.org/10.1021/nl052326h
46. Shekhar, S., Khan, A. M., Sharma, S., Sharma, B. & Sarkar, A. Schiff base metallodrugs in antimicrobial and anticancer chemotherapy applications: a comprehensive review. *Emerg. Mater.* **5**, 279–293. https://doi.org/10.1007/s42247-021-00234-1

Acknowledgements

This work was supported by the Department of Medical Nanotechnology, School of Advanced Medical Sciences and Technologies, Shiraz University of Medical Sciences, Shiraz, Iran. The authors kindly thank the Shiraz University of Medical Sciences for technical assistance.

Author contributions

" S.A. and A.M.A: Writing-original draft preparation, conceptualization, methodology, validation, investigation, formal analysis. A.J and A.Z: Methodology. A.J: Software. Z.Z: Antimicrobial tests, data curation, validation, writing-review and editing. A.V: MTT Test, data curation, writing-review and editing. H.K: Formal analysis, writing-review and editing, data curation. S.R.K., S.M.S and S.C: Formal analysis, writing-review and editing, data curation, resources, visualization. A.M.A, S.C, and S.M.S: Supervision. S.A, A.M.A, A.J and A.Z: Project administration. A.M.A, S.R.K, S.M.S: Funding acquisition."

Declarations

Competing interests

The authors declare no competing interests.

Conflict of interest

The authors declare no conflicts of interest.

Additional information

Correspondence and requests for materials should be addressed to A.M.A. or H.K.